Systematics of first 2^+ state *g* factors around mass 80

T. J. Mertzimekis and A. E. Stuchbery*
National Superconducting Cyclotron Laboratory, Michigan State University, East Lansing, Michigan 48824, USA

N. Benczer-Koller and M. J. Taylor†
Department of Physics and Astronomy, Rutgers University, New Brunswick, New Jersey 08903, USA
(Received 8 May 2003; published 11 November 2003)

The systematics of the first 2^+ state *g* factors in the mass 80 region are investigated in terms of an IBM-II analysis, a pairing-corrected geometrical model, and a shell-model approach. Subshell closure effects at $N=38$ and overall trends were examined using IBM-II. A large-space shell-model calculation was successful in describing the behavior for $N=48$ and $N=50$ nuclei, where single-particle features are prominent. A schematic truncated-space calculation was applied to the lighter isotopes. The variations of the effective boson *g* factors are discussed in connection with the role of *F*-spin breaking, and comparisons are made between the mass 80 and mass 180 regions.

DOI: 10.1103/PhysRevC.68.054304 PACS number(s): 21.10.Ky, 21.60.Cs, 21.60.Fw, 27.50.+e

I. INTRODUCTION

In the past few years the application of the transient-field technique [1] and Coulomb excitation in inverse and normal kinematics has yielded extensive excited-state *g*-factor data with a precision of the order of a few percent. In the $A\sim80$ mass region, low-lying energy states in several isotopes have been measured for the first time or re-measured with higher precision [2–4]. A plethora of interesting effects occurs in this mass region, many of which have been associated with the features of the *g*-factor data [1–5].

Gyromagnetic ratios provide insights into many nuclear structure questions since they are sensitive to contributions from both collective and single-particle degrees of freedom. The main purpose of the present paper is to investigate the *g*-factor systematics in $A\sim80$ nuclei. Starting from an approximate IBM-II formula for the *g* factors of the 2_1^+ states, the systematics in the particular mass region are examined in Sec. II. This initial survey extends and updates that of Wolf *et al.* [6,7] who had fewer and less precise data available at the time. Further insight into the *g*-factor systematics is then sought in Sec. III by applying the pairing-corrected geometrical model (Migdal approximation) to nuclei with more than a few nucleons away from $N=50$. Finally, in Sec. IV, large basis shell-model calculations are performed for nuclei near $N=50$, along with more schematic restricted-basis calculations for the Kr and Se isotopes, in an attempt to provide a global picture of the systematics. Since the *g*-factor systematics should have similar features in the $A=80$ and $A=180$ regions, according to the lowest-order IBM-II formulation, the Discussion places an emphasis on comparisons with—and contrasts between—these two regions.

II. IBM-II AND EFFECTIVE *g* FACTORS

In IBM-II [8], the version of the interacting boson model [9] where protons and neutrons are distinct, the *g* factors of the 2_1^+ states in even-even nuclei are given by a simple relation, provided that the low-excitation states have maximal proton-neutron (*F*-spin) symmetry. Morrison [10] expressed $g(2_1^+)$ in terms of the scalar, g_s, and the vector, g_v, boson *g* factors:

$$g(2_1^+) = g_s + g_v \frac{M_F}{F}, \tag{1}$$

where $g_{s,v}=(g_\pi \pm g_\nu)/2$, $F=F_{\max}=\frac{1}{2}(N_\pi+N_\nu)$ is the *F*-spin, and $M_F=\frac{1}{2}(N_\pi-N_\nu)$ is its projection. The proton and neutron boson numbers N_π and N_ν, respectively, are counted from the nearest closed shell, and g_π and g_ν are the *g* factors of the proton and neutron bosons, respectively. Sambataro *et al.* [11] expressed the *g* factor in an equivalent form

$$g(2_1^+) = g_\pi \frac{N_\pi}{N_\pi+N_\nu} + g_\nu \frac{N_\nu}{N_\pi+N_\nu}. \tag{2}$$

Equations (1) and (2) are exact for *F*-spin symmetric states, as is usually expected for low-excitation states in collective nuclei [12,13]. Thus, if the low-spin states have *F*-spin symmetry, $F=F_{\max}$, their *g* factors are given by Eq. (2) independent of the parameters of the Hamiltonian.

If orbital contributions only are considered, the boson *g* factors are $g_\pi=1$ and $g_\nu=0$, thus giving

$$g(2_1^+) = \frac{N_\pi}{N_\pi+N_\nu}. \tag{3}$$

This expression is analogous to the hydrodynamical model prediction for the *g* factor, $g\approx Z/A$, but $N_\pi/(N_\pi+N_\nu)\approx Z/A$ only if the number of valence nucleons is large. Furthermore, Z/A and $N_\pi/(N_\pi+N_\nu)$ have the opposite dependence on neutron number in the upper half of a shell where the boson number is determined by the number of valence *holes*. This effect is supported by the *g*-factor data in the nuclei below $N=126$, especially in the W and Os isotopes, where the $g(2_1^+)$ values increase with neutron number. A similar difference between the two models occurs in the

*Permanent address: Department of Nuclear Physics, Australian National University, Canberra ACT 0200, Australia.

†Present address: School of Engineering, University of Brighton, Brighton BN2 4GJ, UK

$A=80$ region as the neutron number approaches $N=50$.

For heavier masses ($A\sim150-190$), both IBM-II and collective model predictions have been tested experimentally [14,15] showing that, in the majority of the cases, IBM-II better describes the g factors in the upper half of the shell near $A=180$. Wolf *et al.* [6,7] investigated effective g factors in a broad range of masses by treating g_π and g_ν as free parameters and fitting experimental data. In the mass 180 region they obtained $g_\pi=0.63(4)$ and $g_\nu=0.05(5)$ [6,7].

To survey the g-factor data in the mass 80 region, Eq. (2) can be rearranged into a form which is linear to the ratio N_π/N_ν:

$$g(2_1^+)\left(\frac{N_{tot}}{N_\nu}\right)=g_\pi\left(\frac{N_\pi}{N_\nu}\right)+g_\nu, \tag{4}$$

where $N_{tot}=N_\pi+N_\nu$. The parameter g_π now represents the slope of a straight line and g_ν is the corresponding intercept. As will be seen below, Eq. (4) is very useful for displaying global systematics in the data. However, because the g factor is multiplied by (N_{tot}/N_ν) in the plots, the details of the variations in the g factors as a function of proton and neutron numbers tend to be hidden.

In the light of the new, precise measurements that have been performed recently in the $A\sim80$ mass region, the IBM-II fit was revisited focusing particularly on the systematics of the even-even isotopes with $28<Z<40$. The present analysis includes a complete set of measured g factors of the 2_1^+ states in stable isotopes in the 28–40 proton shell. Recent measurements exist for $_{30}$Zn [2], $_{34}$Se [3], and $_{36}$Kr [4] isotopes. Weighted averages were used in case older data existed [5,16–18]. The data are summarized in Table I.

Discontinuities in g-factor systematics may occur for proton and/or neutron subshell closures. Thus, along with boson counting from the usual shell gaps for protons and neutrons at 28 and 50, separate evaluations were performed which considered the rather well-established closed proton subshell at $Z=40$ and the neutron subshell closure at $N=38$, as suggested in an IBM-II study of the g factors in the Se isotopes [3]. In all, there are four alternative ways of counting the bosons. A corresponding set of g_π and g_ν values was obtained for each case. The fits are illustrated in Figs. 1 and 2, and the results are summarized in Table II. Data points corresponding to isotopes at closed (sub) shells and the data of the $N=48$ isotones were excluded from the fits because these nuclei show clear departures from the collective values observed for $N\leqslant46$.

The introduction of a proton subshell closure at $Z=40$ has no significant effect on either the quality of the fit or the boson g factor values, as is evident in both figures and Table II. On the other hand, the introduction of the $N=38$ neutron subshell closure results in a change of the deduced effective values, bringing them closer to the bare values and improving χ^2 significantly. Specifically, when the neutron shell closure is turned on, the proton effective g factor increases by $\approx8\%$, while the neutron g factor becomes smaller by $\approx16\%$. For the following discussion the fit with protons in the $28<Z<50$ shell and the neutrons in $38<N<50$ is used. The effective boson g factors for this case are $g_\pi=0.435(8)$ and $g_\nu=0.356(7)$, corresponding to the fit in Fig. 2(a). The marked deviation of these effective values of g_π and g_ν from 1 and 0, respectively, is difficult to reconcile with microscopic expectations. This problem will be discussed below.

TABLE I. Experimental g factors for $28<Z<50$. The data correspond to weighted averages of recent and older data. Closed proton shell nuclei are not displayed ($_{28}$Ni, $_{40}$Zr).

Isotope	Z	N	$g(2_1^+)$
		32	0.371(99)
Zn	30	34	0.445(46)
		36	0.399(41)
		38	0.436(47)
		40	0.378(42)
		38	0.459(23)
Ge	32	40	0.386(27)
		42	0.400(15)
		44	0.383(20)
		40	0.428(27)
Se	34	42	0.403(23)
		44	0.384(25)
		46	0.435(27)
		48	0.496(29)
		42	0.432(27)
Kr	36	44	0.378(47)
		46	0.402(15)
		48	0.267(13)
		50	1.12(14)
		46	0.419(47)
Sr	38	48	0.273(50)
		50	1.15(17)

It was noted above that plots of $g(2_1^+)N_{tot}/N_\nu$ versus N_π/N_ν can sometimes visually suppress the differences between the global fit and the experimental data. For this reason, the predicted g factors from the adopted "best" fit are compared with the experiment in Fig. 3 along with "benchmark" IBM-II predictions for $g_\pi=1$ and $g_\nu=0$ and the results of the pairing-corrected hydrodynamical model to be described in the following section.

III. THE MIGDAL APPROXIMATION

The IBM-II fits presented in the preceding section, for nuclei in the mass 80 region with $N\leqslant46$, yielded $g_\pi\approx g_\nu\approx0.4$. This condition implies that $g(2^+)\approx0.4\approx Z/A$ for all nuclei included in the fit and stimulates an examination of the systematics in terms of the hydrodynamical collective model.

In this model the g factor of a collective state is $g\sim Z/A$ whether the state is considered vibrational, rotational, or intermediate between these limits. The most important correction to the Z/A estimate originates from differences in pairing correlations for the moment of inertia of the proton and neutron "fluids" ($\mathcal{J}_{p,n}$):

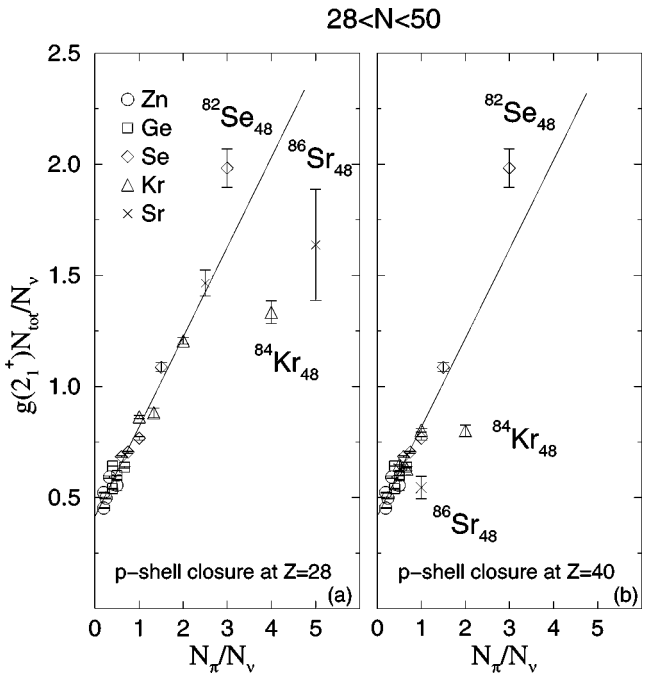

FIG. 1. Fit of the experimental data for the case when no neutron subshell closure at N=38 was considered and neutron bosons are counted within the 28–50 shell. Left: proton bosons are counted within the 28–50 shell. Right: proton boson counting is altered due to the proton subshell closure at Z=40. Data for the N=48 isotones are not included in the fits.

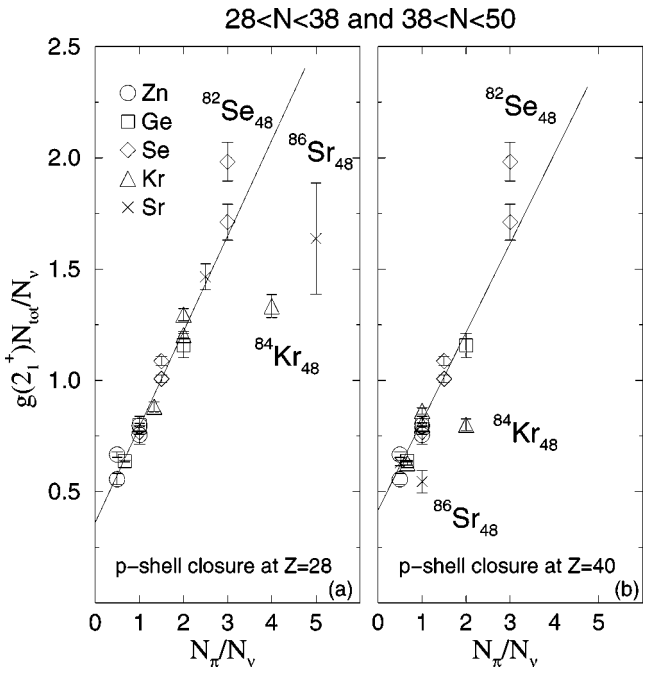

FIG. 2. Fit of the experimental data for the case when a neutron subshell closure at N=38 was considered. Left: no proton subshell closure. Right: proton subshell closure at Z=40 was included in the analysis. Data for the N=48 isotones are not included in the fits. The quality of the fit in both panels is better than for the corresponding fits in Fig. 1.

$$g = \frac{\mathcal{J}_p}{\mathcal{J}_p + \mathcal{J}_n}. \tag{5}$$

A simple and successful method of estimating these corrections for nuclei in the $A \sim 150-180$ [14] and the $A \sim 100$ regions [19] is provided by the Migdal approximation [20]. The collective g factor is given by

$$g = \frac{Z\mathcal{J}(A, \delta, \Delta_p)}{Z\mathcal{J}(A, \delta, \Delta_p) + N\mathcal{J}(A, \delta, \Delta_n)}, \tag{6}$$

where δ is the deformation and Δ_p and Δ_n are the pair gaps for protons and neutrons, respectively. $\mathcal{J}(A, \delta, \Delta)$ is the moment of inertia evaluated in the Migdal approximation as described in Ref. [14], and references therein. The moment of inertia is expressed as the sum of two terms $\mathcal{J}_1$ and $\mathcal{J}_2$. The former is dominant and originates from the $\Delta N=0$ Coriolis coupling, while the latter makes a small correction for Y_{21} quadrupole pairing and Coriolis coupling between oscillator shells with $\Delta N=2$ (see Ref. [14] for details). The present calculations included both $\mathcal{J}_1$ and $\mathcal{J}_2$ terms in the evaluation of g factors. Deformations were taken from intrinsic quadrupole moments Q_0 determined from experimental $B(E2)$ data [21] and pair gaps were evaluated as 80% of the relevant odd-even mass differences [22]. In these near-spherical nuclei the deformations determined from $B(E2)$ data may not be very accurate. However, the sensitivity of the g factor to $\Delta_{p,n}$ and δ has been examined in Ref. [14]. Generally, the g factor is not very sensitive to the deformation, but depends sensitively on the magnitudes—especially the relative magnitudes—of the pair gaps. Uncertainties in the assumed deformations are therefore not expected to have a large impact on the calculated g-factor systematics. The parameters of the analysis appear in Table III and the results are compared with the experimental data in Fig. 3.

There is an overestimation of the g factors for the case of Zn and Ge isotopes, by a factor of 10–20%. Apart from this tendency, the agreement between theory and experiment is good. As with the IBM-II fit, the g factors of the N=48 isotones show strong departures from collective behavior and these are discussed in the following section.

IV. SHELL-MODEL CALCULATIONS

A. Previous work

A number of shell-model calculations have been reported for the mass region above and below ^{90}Zr. Calculations of the theoretical magnetic moments in the Zr and Mo isotopes

TABLE II. Effective values of g_π and g_ν for different ways of counting proton and neutron bosons, $28<Z<40$.

Mass	Z	N	g_π	g_ν	χ^2
$A \sim 80$	28–50	28–50	0.404(4)	0.414(2)	172.02
	28–50	38–50	0.435(8)	0.356(7)	8.83
	28–40	28–50	0.400(4)	0.417(2)	177.8
	28–40	38–50	0.432(10)	0.364(9)	11.02

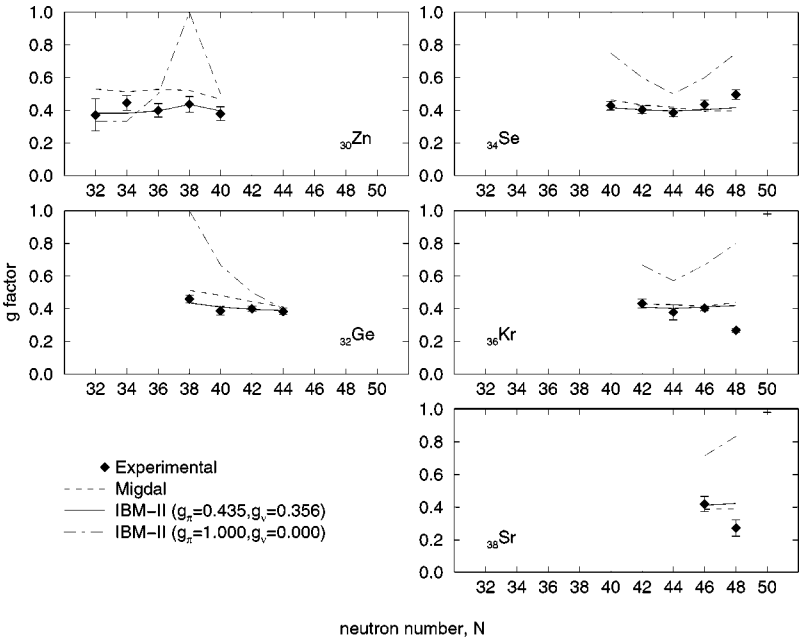

FIG. 3. Experimental (diamonds), IBM-II (solid and dot-dashed lines), and pairing-corrected (dashed lines) g factors of the 2_1^+ states.

with $N>50$ have been presented recently in Refs. [19,23–25] (these papers include references to earlier related work). High-spin states have been studied extensively for nuclei with $Z\sim40-44$ and $N\sim46-50$ through shell-model calculations which included the evaluation of g factors (see Refs. [26,27], and references therein). Nuclei below $Z=40$ and $N=50$ have been studied less thoroughly, particularly in relation to the g factors of low-excitation states. Reference [28] contains information on calculations of binding energies and other properties of nuclei in the lower fp shell. Results of calculations in the upper fp shell, mainly focused on energy levels and $B(E2)$s, are reported in Ref. [29], and references therein. Ji and Wildenthal [30] have determined effective interactions in the $Z=32-46$, $N=50$ nuclei; Warburton *et al.* [31] have investigated the role of the two neutron holes in the $g_{9/2}$ shell in ^{86}Sr; and earlier, Fields *et al.* [32] have suggested a configuration for the 2_1^+ state in the same nucleus. There also exist shell-model calculations [33] in the lower fp shell, which focus on the lighter isotopes around $Z,N=28$.

TABLE III. Parameters and results of the pairing-corrected hydrodynamical model calculations. δ is the deformation and $\Delta_{p/n}$ is the pair gap of protons/neutrons. The right column shows the predicted g factors of the Migdal approximation, g_{MA}.

Nucleus	Z	A	δ	Δ_p (keV)	Δ_n (keV)	g_{MA}
		62	0.181	1069	1291	0.527
Zn	30	64	0.199	1072	1326	0.510
		66	0.182	1026	1418	0.524
		68	0.171	962	1372	0.516
		70	0.189	957	1223	0.464
		70	0.186	1166	1493	0.510
Ge	32	72	0.199	1188	1460	0.479
		74	0.227	1251	1422	0.441
		76	0.213	1181	1256	0.411
		74	0.241	1445	1549	0.463
Se	34	76	0.245	1369	1373	0.432
		78	0.220	1297	1323	0.420
		80	0.192	1252	1232	0.395
		82	0.163	1136	1205	0.399
		78	0.273	1416	1258	0.428
Kr	36	80	0.215	1409	1364	0.425
		82	0.170	1317	1319	0.415
		84	0.129	1140	1291	0.438
		86	0.126	1064	1416	0.479
		84	0.179	1524	1305	0.389
Sr	38	86	0.122	1295	1206	0.391
		88	0.103	1107	1487	0.508

B. Details of the calculations

Full-space calculations in the fp and g shells near $A=80$ are limited by the large model space required for a complete analysis. In the present study large-basis calculations for the $N=48,50$ isotones were performed first. Then, for $N=40-46$, a set of calculations with very truncated basis spaces was carried out to study the qualitative differences in the g-factor behavior for the Se and Kr isotopes.

Calculations were performed using the code OXBASH [34] and the "GWB" basis with the "GWBXG" interactions. The core is ^{56}Ni and the full basis space available is $\pi(1f_{5/2},2p_{3/2},2p_{1/2},1g_{9/2})$ and $\nu(1g_{9/2},2p_{1/2},2d_{5/2},3s_{1/2},2d_{3/2},1g_{7/2})$. Since $N\leqslant50$ nuclei are considered here, only the $\nu1g_{9/2}$ and $\nu2p_{1/2}$ orbits are active in the neutron space. For practical calculations there must be further restrictions on the allowed configurations. In the calculations performed for $N=48,50$ the proton excitations were constrained by the requirements that (i) no more than two protons can be excited across the $Z=40$ subshell gap into $\pi1g_{9/2}$ and (ii) the occupation of the $\pi1f_{5/2}$ cannot be less than two. For the

TABLE IV. Configuration spaces used in shell-model calculations. The allowed occupations of the single-particle orbits are indicated.

N	Protons				Neutrons	
	$1f_{5/2}$	$2p_{3/2}$	$2p_{1/2}$	$1g_{9/2}$	$2p_{1/2}$	$1g_{9/2}$
50	2–6	0–4	0–2	0–2	2	8
48	2–6	0–4	0–2	0–2	0–2	6–8
46	2–6	0–4	0–2	0	2	6
44	2–6	0–4	0–2	0	2	4
42	2–6	0–4	0–2	0	0–2	0–4
40	2–6	0–4	0–2	0	0–2	0–2

schematic study of nuclei with $N<48$ no proton excitations were allowed across the $Z=40$ subshell gap (i.e., the $\pi 1g_{9/2}$ was not occupied) and it was required that the occupation of the $\pi 1f_{5/2}$ orbit not be less than two. For $N=44, 46$ full occupation of the $\nu 2p_{1/2}$ orbit was enforced, but this restriction was not imposed for $N=40, 42$. The configuration spaces are summarized in Table IV.

The GWBXG residual interaction combines effective interactions from the bare G matrix of the H7B potential [35] with empirically adjusted matrix elements and single-particle energies. Further details are provided in Refs. [36,37] and with the OXBASH distribution [34]. Of particular relevance, the interaction includes the proton-proton interaction determined by Ji and Wildenthal for the $1f_{5/2}$, $2p_{3/2}$, $2p_{1/2}$, and $1g_{9/2}$ orbits in $N=50$ nuclei. The single-particle energies are optimized for $A\sim 90$, near the upper end of the mass range of present interest, but no attempt was made to fine tune them for this initial survey of the low-spin magnetic moments.

The excitation energy $E(2_1^+)$ and the reduced transition rate $B(E2;2_1^+\rightarrow 0_1^+)$ have also been calculated, along with the g factor of the 2_1^+ state. Together with the g factors, these observables give an indication of the relative contributions of single-particle and collective components in the 2_1^+ state wave function. However, the shell-model calculations tend to underestimate the collective components, especially where the basis space is severely truncated.

As in the previous work on the Zr and Mo isotopes [19,25], the effective charges of the proton and neutron were taken to be $e_\pi^{\rm eff}=1.77$ and $e_\nu^{\rm eff}=1.19$ and the intrinsic spin g factors were quenched to 0.75 times the bare nucleon values, i.e., $g_s(\pi)=+4.19$, $g_s(\nu)=-2.87$, while the orbital g factors were $g_l=1(0)$ for protons(neutrons). The g factors of the relevant single-particle orbits are summarized in Table V.

TABLE V. Single-nucleon g factors near $Z=40$ and $N=50$ with $g_{eff}=0.75g_s^{bare}$.

Protons		Neutrons	
$\pi 1f_{5/2}$	+0.544	$\nu 2p_{1/2}$	+0.956
$\pi 2p_{3/2}$	+2.063	$\nu 1g_{9/2}$	−0.319
$\pi 2p_{1/2}$	−0.063		
$\pi 1g_{9/2}$	+1.354		

C. Shell-model results

Results of the calculations are presented in Table VI. Generally the energies of the 2_1^+ states are well reproduced, as are the $B(E2;2_1^+\rightarrow 0_1^+)$ values. Clear discrepancies in these observables begin to show only for the Sr and Kr isotones with $N\leqslant 44$. The following sections discuss the g-factor trends which are displayed in Figs. 4 and 5.

1. N=50

The $g(2_1^+)$ values in the $N=50$ isotones are very well reproduced. As can be seen from the wave functions in Table VII and the tabulated single-particle g factors (Table V), the gradual increase in g factor between Se and Sr is associated with the rise in the Fermi surface which gives increasing emphasis to configurations involving the $\pi p_{3/2}$ orbit.

2. N=46, 48

In the $N=48$ isotones the calculated $g(2_1^+)$ values follow the experimental trend, but are all shifted by about −0.2. The underestimation of the g factors in the $N=46$ isotones is even greater, a point discussed further in Sec. V. It has been noted previously that the experimental g factors of 2^+ states near closed neutron shells are displaced somewhat from the shell-model values in the direction of the collective estimate Z/A [19,23,38–40]. The present results for the $N\leqslant 48$ isotones also show this trend. Theory and experiment could be brought into better agreement for $N=48$ by increasing the strength of the proton-neutron interactions, but it is beyond the scope of the present work to attempt such tuning. There may also be contributions from proton excitations deeper in the core as collectivity sets in. For the present purposes it is sufficient to note that the 2_1^+ states in the $N=48$ isotones have strong neutron contributions and that these are most pronounced when there are only a few valence proton holes. As the number of proton holes increases the states become more symmetric with respect to proton and neutron excitations as is seen by the increase in $g(2_1^+)$ in both theory and experiment between, say, ^{84}Kr and ^{82}Se. The implications of this inference for the systematics and IBM fit will be discussed in Sec. V.

3. g-factor trends in the Kr and Se isotopes with N≤46

The experimental and theoretical g factors for the Se and Kr isotopes are compared in Fig. 5. For this presentation 0.2 has been added to the theoretical values. The purpose of this diagram is to compare the mass-dependent trends in the experimental and theoretical g factors of the Kr and Se isotopes, particularly for $N\leqslant 46$. It is interesting to note that, while the magnitudes of the g values are very much underestimated, the predicted mass variation for the isotopes with $N=42, 44, 46$ is different for Se and Kr, and the qualitative trend is in agreement with the experiment. Furthermore, the shell-model calculations for the Se isotopes show the trend predicted by the IBM and observed in experiment, namely, the smallest $g(2^+)$ value occurs for the $N=44$ nucleus ^{78}Se, where the valence neutron shell $(2p_{1/2}\otimes 1g_{9/2})$ is half filled. In contrast, but again in agreement with experimental trends,

TABLE VI. Shell-model calculations of g factors, $B(E2)$s, and excitation energies of 2_1^+ states in the $N=50$ and $N=48$ isotones. The energies are in keV and the $B(E2)$s are in e^2 fm^4. Data are from Refs. [21,24,41,42].

	Nuclide	Quantity	Theory	Experiment
$N=50$	$^{84}_{34}Se_{50}$	E_x	1685	1455
		g	+0.824	
		$B(E2;2_1^+\rightarrow 0_1^+)$	245	
	$^{86}_{36}Kr_{50}$	E_x	1504	1565
		g	+0.988	+1.12(14)
		$B(E2;2_1^+\rightarrow 0_1^+)$	180	244(20)
	$^{88}_{38}Sr_{50}$	E_x	1981	1836
		g	+1.141	+1.15(17)
		$B(E2;2_1^+\rightarrow 0_1^+)$	133	184(1)
$N=48$	$^{82}_{34}Se_{48}$	E_x	738	655
		g	+0.296	+0.496(29)
		$B(E2;2_1^+\rightarrow 0_1^+)$	496	364(10)
	$^{84}_{36}Kr_{48}$	E_x	896	882
		g	+0.054	+0.267(13)
		$B(E2;2_1^+\rightarrow 0_1^+)$	380	250(12)
	$^{86}_{38}Sr_{48}$	E_x	1009	1077
		g	−0.117	+0.273(50)
		$B(E2;2_1^+\rightarrow 0_1^+)$	279	256(28)
$N=46$	$^{80}_{34}Se_{46}$	E_x	426	666
		g	+0.114	+0.435(27)
		$B(E2;2_1^+\rightarrow 0_1^+)$	655	506(12)
	$^{82}_{36}Kr_{46}$	E_x	608	776
		g	−0.057	+0.402(15)
		$B(E2;2_1^+\rightarrow 0_1^+)$	497	446(20)
	$^{84}_{38}Sr_{46}$	E_x	662	793
		g	−0.084	+0.419(47)
		$B(E2;2_1^+\rightarrow 0_1^+)$	408	578(88)
$N=44$	$^{78}_{34}Se_{44}$	E_x	507	614
		g	+0.070	+0.384(25)
		$B(E2;2_1^+\rightarrow 0_1^+)$	589	670(18)[a]
	$^{80}_{36}Kr_{44}$	E_x	595	617
		g	−0.056	+0.378(47)
		$B(E2;2_1^+\rightarrow 0_1^+)$	516	740(42)
	$^{82}_{38}Sr_{44}$	E_x	531	574
		g	−0.094	
		$B(E2;2_1^+\rightarrow 0_1^+)$	419	1026(40)
$N=42$	$^{76}_{34}Se_{42}$	E_x	737	559
		g	+0.125	+0.403(23)
		$B(E2;2_1^+\rightarrow 0_1^+)$	534	840(20)
	$^{78}_{36}Kr_{42}$	E_x	905	455
		g	+0.066	+0.378(47)
		$B(E2;2_1^+\rightarrow 0_1^+)$	467	1266(78)
	$^{80}_{38}Sr_{42}$	E_x	906	386
		g	−0.013	
		$B(E2;2_1^+\rightarrow 0_1^+)$	467	1918(72)
$N=40$	$^{74}_{34}Se_{40}$	E_x	718	634
		g	+0.239	+0.428(27)
		$B(E2;2_1^+\rightarrow 0_1^+)$	430	774(16)

[a]A recent measurement [43] has yielded a value of 650(90) e^2 fm^4.

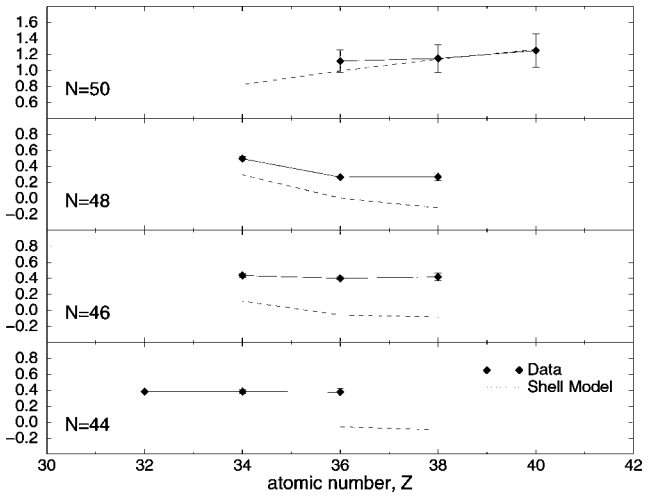

FIG. 4. Experimental $g(2_1^+)$ values (diamonds) vs shell-model predictions (dashed lines) for $N=44, 46, 48$, and 50.

the shell-model calculations predict that the $N=44$ and $N=46$ isotopes of Kr have nearly equal g factors, with no clear "midshell minimum."

V. DISCUSSION

There are three features of the g-factor data in the mass 80 region to address: (i) The clear departures of the $g(2^+)$ values in nuclei with $N=48$ from the collective values observed for $N\leqslant 46$. (ii) The departures of the effective boson g factors from their "bare" values. (iii) Similarities and differences between the mass 80 region, where $g_\pi \approx g_\nu \approx 0.4$, and the mass 190 region, where $g_\pi \approx 1$ and $g_\nu \approx 0$.

(i) The g-factor calculations and comparisons with experiment in the previous sections have shown that the nuclei in the mass 80 region have strong single-particle characteristics for $N=48$ and $N=50$ and then show a transition to collective values for $N\leqslant 46$. In particular, the g factors show a rapid

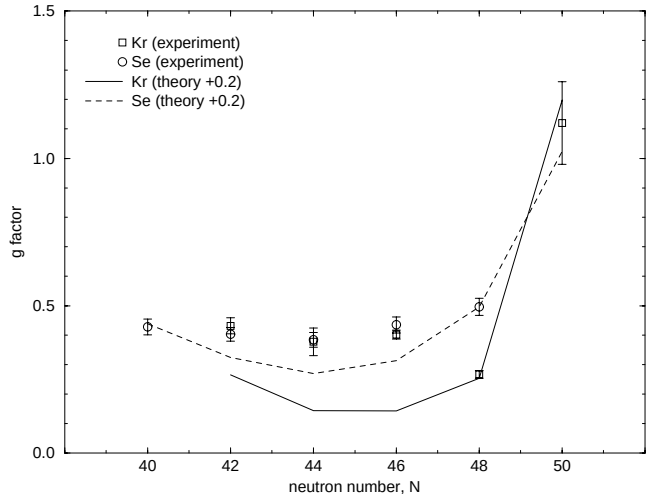

FIG. 5. Experimental $g(2_1^+)$ values vs shell-model predictions for the Kr and Se isotopes. For this presentation 0.2 has been added to all of the theoretical g factors.

TABLE VII. Theoretical wave functions of 2_1^+ states.

Nuclide	Dominant partitions
$^{84}_{34}Se_{50}$	$61\%\|\pi f_{5/2}^4 p_{3/2}^2 p_{1/2}^0 g_{9/2}^0 \otimes \nu p_{1/2}^2 g_{9/2}^{10}\rangle + \cdots$
$^{86}_{36}Kr_{50}$	$37\%\|\pi f_{5/2}^6 p_{3/2}^2 p_{1/2}^0 g_{9/2}^0 \otimes \nu p_{1/2}^2 g_{9/2}^{10}$
	$+26\%\|\pi f_{5/2}^6 p_{3/2}^1 p_{1/2}^1 g_{9/2}^0 \otimes \nu p_{1/2}^2 g_{9/2}^{10}\rangle + \cdots$
$^{88}_{38}Sr_{50}$	$83\%\|\pi f_{5/2}^6 p_{3/2}^3 p_{1/2}^1 g_{9/2}^0 \otimes \nu p_{1/2}^2 g_{9/2}^{10}\rangle + \cdots$
$^{82}_{34}Se_{48}$	$53\%\|\pi f_{5/2}^4 p_{3/2}^2 p_{1/2}^0 g_{9/2}^0 \otimes \nu p_{1/2}^2 g_{9/2}^8\rangle + \cdots$
$^{84}_{36}Kr_{48}$	$32\%\|\pi f_{5/2}^6 p_{3/2}^2 p_{1/2}^0 g_{9/2}^0 \otimes \nu p_{1/2}^2 g_{9/2}^8$
	$+17\%\|\pi f_{5/2}^6 p_{3/2}^1 p_{1/2}^1 g_{9/2}^0 \otimes \nu p_{1/2}^2 g_{9/2}^8\rangle + \cdots$
$^{86}_{38}Sr_{48}$	$32\%\|\pi f_{5/2}^6 p_{3/2}^4 p_{1/2}^0 g_{9/2}^0 \otimes \nu p_{1/2}^2 g_{9/2}^8\rangle + \cdots$

change from values that are clearly associated with single-particle structures to values that would nominally be associated with collectivity. The present shell-model calculations are able to track the qualitative behavior of the g factors between $N=50$, where the first 2^+ states are dominated by fp-shell proton excitations, and $N=48$, where the valence neutron configuration becomes dominant, but cannot describe the onset of collective g factor values at $N=46$. Nevertheless, a vestige of the shell-model structure appears to persist in the apparently collective excitations in the isotopes of Se and Kr having $N=42-46$, and the $E(2_1^+)$ and $B(E2)$ values remain reasonably well described at $N=46$ despite the poor description of the g factors.

(ii) Since boson g factors that depart significantly from the "bare" values, $g_\pi=1$, $g_\nu=0$, cannot be justified in realistic IBM calculations, F-spin breaking must be invoked to explain the mass 80 g-factor data. Indeed empirical IBM-II fits to the g-factor data can be obtained, without greatly disturbing the fits to other observables, by allowing the single-particle energies of the proton and neutron bosons (ϵ_π and ϵ_ν) to differ [3,4,44]. The shell-model calculations suggest that there might be a microscopic justification for this procedure.

In nuclei with only a few valence nucleons the proton and neutron configurations tend to be weakly coupled, with a dominance of neutron excitations in the lowest 2^+ state. This behavior, which is evident from both shell-model calculations and comparisons of experimental data, has been discussed in several recent publications [19,23,37–40]. Unfortunately, when more than a few valence nucleons are added it is impossible to track the coupling of the proton and neutron spaces via conventional shell-model calculations. Nevertheless the experimental data, especially the g-factor data, and schematic calculations, such as those for the Se and Kr isotopes presented above, imply that the proton and neutron spaces become more strongly coupled as the number of valence nucleons increases and collectivity sets in.

From the perspective of the IBM, these observations suggest that the proton-neutron (or F-spin) symmetry is broken rather strongly in nuclei with few valence proton bosons, and the symmetry breaking increases in those isotopes that approach the neutron shell closure. Furthermore, the shell-model calculations seem to be consistent with a mechanism whereby the neutron boson energy ϵ_ν becomes significantly smaller than the proton boson energy ϵ_π as the closed neutron shell is approached. These conclusions are consistent with recent studies in nuclei with $N=52$ where the lowest mixed-symmetry states (having $F=F_{\max}-1$) have been identified and investigated through shell-model calculations. For example, Werner *et al.* [45] have noted that while the second 2^+ state in ^{92}Zr shows the signatures of the mixed-symmetry state, the first 2^+ state is almost a pure neutron configuration, in contradiction with the F-spin symmetric limit.

Since the boson number is small throughout the mass 80 region, it is reasonable to suggest that the g factors in the mass 80 region do not show the simple IBM-II type of behavior [required by Eq. (3) and indicated by the dot-dashed line in Fig. 3] because isotopes do not exist near mass 80 with sufficient protons and neutrons to form a system of interacting bosons with F-spin symmetry. Of those that have been studied the isotopes of Se, which have both proton and neutron occupation near the middle of the valence shell, best satisfy this requirement, and are indeed the only cases where the behavior prescribed by Eq. (3) is at all manifested, if at all, in the experimental data.

(iii) At first sight, the g-factor systematics in the $A=80$ and $A=180$ regions seem very different, despite the expectation of similarities stemming from the fact that in both regions neutrons occupy the upper part of the respective valence shell. Partly, this perception stems from the limitation of the data to stable isotopes, but more importantly, the significant difference in the neutron boson numbers for the two regions must have consequences, according to the discussion in the preceding paragraphs.

The pairing-corrected hydrodynamical model in Sec. III is very successful in describing the $A=80$ experimental data, most of which apply to nuclei below the neutron mid shell. However, it can be expected that clear discrepancies might appear if more data for collective isotopes with $N>44$ existed, as indeed this model fails for the W, Os and Pt isotopes in the $A=190$ region [14].

Returning to the discussion in terms of the shell model and the IBM, the comparisons of theory and experiment for the Se and Kr isotopes (six and four valence proton holes, respectively) suggest a more specific analogy with the behavior of the g factors of the 2_1^+ states in the Os and Pt isotopes near $A=190$ (also having six and four valence proton holes, respectively). The g factors of the Os isotopes follow the IBM-II prediction with $g_\pi \sim 1$ and $g_\nu \sim 0$ whereas the Pt isotopes have nearly constant g factors with $g_\pi \sim g_\nu \sim 0.3$. This empirical behavior of the Os and Pt isotopes seems to be echoed in the Sr and Kr isotopes.

The $M1$ behavior of the ^{188,190,192}Os and ^{190,192,194,196,198}Pt isotopes has been examined in detail in terms of F-spin mixing in the IBM-II [46,47], but without an understanding of the underlying microscopic structure or why different F-spin breaking mechanisms are needed for the Os and Pt isotopes. Putting together the above observations on the mass 190 region and the present study of the mass 80 region, one can conjecture that F-spin symmetry breaking is very sensitive to the number of valence nucleons when the boson number is small, and that this effect can give rise to strikingly different g-factor trends for adjacent isotope chains in a transitional region. Further theoretical investigations are needed to connect these qualitative observations based on shell-model calculations to the microscopic basis for the IBM. Some work

along these lines has already been performed for the $Z=50-82$ and $N=82-126$ shells [48].

Finally, the $g(2_1^+)$ values have been measured [15,47,49,50] for the Pt isotopes between ^{180}Pt and ^{198}Pt and found to remain remarkably constant. While F-spin mixing mechanisms can explain the constancy of the g factors of the oblate nuclei with $A \geqslant 190$, the g factors of the isotopes with $A<190$ are evidently strongly affected by the transition to prolate-deformed ground-state bands in the Pt isotopes around mass 182, which are associated with shape coexistence and a deformation-driving intruder configuration. In terms of IBM-II, the intruder configuration has two more proton bosons than the normal configuration, which brings the g factors of the 2_1^+ states near the middle of the valence neutron shell closer to Z/A. As a generalization, it would be expected that intruder states which drive shape changes in the mass 80 region will also influence the g factors. For low-spin states in even-even nuclei the main effect (on the g factors) of a configuration which leads to deformed states would be to increase the effective number of nucleons which participate in the nuclear excitation, and thereby to bring g closer to Z/A. Thus for the present discussion of the $g(2_1^+)$ data it has been possible to use the terminology of shape transitions rather than shape coexistence. A specific focus on the influence of intruder states and coexistence may be required when the experimental dataset is expanded to include additional excited states and a wider range of nuclei.

VI. SUMMARY AND CONCLUSIONS

In summary, the $g(2_1^+)$ systematics in the $A=80$ region have been considered in terms of the interacting boson model, a pairing-corrected collective model, and the shell model. The nuclei show transitional structures and a complex interplay of single-particle and collective features. The IBM-II fits imply substantial breaking of the symmetry between proton and neutron bosons, a feature that seems to be correlated with the weak coupling of proton and neutron excitations near closed shells, together with a favoring of the neutron excitations in the lowest states, as implied by shell-model calculations. It is suggested that the g-factor systematics in the mass 80 region have features in common with the behavior of g factors in heavier transitional regions, but the similarities in the empirical g-factor systematics are suppressed because the mass 80 region has many fewer valence nucleons.

ACKNOWLEDGMENTS

This work was supported in part by NSF research Grant Nos. PHY99-83810 and PHY00-98800.

[1] N. Benczer-Koller, M. Hass, and J. Sak, Annu. Rev. Nucl. Part. Sci. **30**, 53 (1980).
[2] O. Kenn, K.-H. Speidel, R. Ernst, S. Schielke, S. Wagner, J. Gerber, P. Maier-Komor, and F. Nowacki, Phys. Rev. C **65**, 034308 (2002).
[3] K.-H. Speidel, N. Benczer-Koller, G. Kumbartzki, C. Barton, A. Gelberg, J. Holden, G. Jakob, N. Matt, R. H. Mayer, M. Satteson, R. Tanczyn, and L. Weissman, Phys. Rev. C **57**, 2181 (1998).
[4] T. J. Mertzimekis, N. Benczer-Koller, J. Holden, G. Jakob, G. Kumbartzki, K.-H. Speidel, R. Ernst, A. Macchiavelli, M. McMahan, L. Phair, P. Maier-Komor, A. Pakou, S. Vincent, and W. Korten, Phys. Rev. C **64**, 024314 (2001).
[5] A. I. Kurcharska, J. Billowes, and M. A. Grace, J. Phys. G **14**, 65 (1988).
[6] A. Wolf, D. D. Warner, and N. Benczer-Koller, Phys. Lett. **158B**, 7 (1985).
[7] A. Wolf and R. F. Casten, Phys. Rev. C **36**, 851 (1987).
[8] T. Otsuka, A. Arima, F. Iachello, and I. Talmi, Phys. Lett. **76B**, 139 (1978).
[9] A. Arima and F. Iachello, Phys. Rev. Lett. **35**, 1069 (1975); Ann. Phys. (N.Y.) **99**, 253 (1976).
[10] I. Morrison, Aust. J. Phys. **33**, 801 (1981).
[11] M. Sambataro, O. Scholten, A. E. L. Dieperink, and G. Piccitto, Nucl. Phys. **A423**, 333 (1984).
[12] M. Sambataro and A. E. L. Dieperink, Phys. Lett. **107B**, 249 (1981).
[13] A. Wolf, O. Scholten, and R. F. Casten, Phys. Lett. B **312**, 372 (1993).
[14] A. E. Stuchbery, Nucl. Phys. **A589**, 222 (1995).
[15] A. E. Stuchbery, S. S. Anderssen, A. P. Byrne, P. M. Davidson, G. D. Dracoulis, and G. J. Lane, Phys. Rev. Lett. **76**, 2246 (1996).
[16] A. Pakou, J. Billowes, J. Burde, J. A. G. de Raedt, M. A. Grace, and W. R. Kolbl, J. Phys. G **10**, 1759 (1984).
[17] G. J. Lampard, H. H. Bolotin, A. E. Stuchbery, C. E. Doran, and A. P. Byrne, Aust. J. Phys. **40**, 117 (1987).
[18] N. J. Stone (unpublished).
[19] P. F. Mantica, A. E. Stuchbery, D. E. Groh, J. I. Prisciandaro, and M. P. Robinson, Phys. Rev. C **63**, 034312 (2001).
[20] A. B. Migdal, Nucl. Phys. **13**, 655 (1959).
[21] S. Raman, C. W. Nestor, Jr., and P. Tikkanen, At. Data Nucl. Data Tables **78**, 1 (2001).
[22] R. Bengtsson, S. Frauendorf, and F.-R. May, At. Data Nucl. Data Tables **35**, 15 (1986).
[23] A. E. Stuchbery, Nucl. Phys. **A682**, 470c (2001).
[24] G. Kumbartzki, N. Benczer-Koller, J. Holden, G. Jakob, T. J. Mertzimekis, M. J. Taylor, K.-H. Speidel, R. Ernst, A. E. Stuchbery, C. W. Beausang, and R. Krücken, Phys. Lett. B **562**, 193 (2003).
[25] A. E. Stuchbery, N. Benczer-Koller, G. Kumbartzki, and T. J. Mertzimekis (unpublished).
[26] D. Rudolph and K. P. Lieb, Nucl. Phys. **A597**, 298 (1996).
[27] E. Galindo, A. Jungclaus, and K. P. Lieb, Eur. Phys. J. A **9**, 439 (2000).
[28] E. Caurier, G. Martinez-Pinedo, F. Nowacki, A. Poves, J. Retamosa, and A. P. Zuker, Phys. Rev. C **59**, 2033 (1999).
[29] E. Caurier, F. Nowacki, and A. Poves, Eur. Phys. J. A **15**, 145

(2002).
[30] X. Ji and B. H. Wildenthal, Phys. Rev. C **37**, 1256 (1988).
[31] E. K. Warburton, J. W. Olness, C. J. Lister, J. A. Becker, and S. D. Bloom, J. Phys. G **12**, 1017 (1986).
[32] C. A. Fields, F. W. N. de Boer, and J. Sau, Nucl. Phys. **A398**, 512 (1983).
[33] D. R. Semon, M. C. Allen, H. Dejbakhsh, C. A. Gagliardi, S. E. Hale, J. Jiang, L. Trache, R. E. Tribble, S. J. Yennello, H. M. Xu, X. G. Zhou, and B. A. Brown, Phys. Rev. C **53**, 96 (1996).
[34] A. Etchegoyen, W. D. Rae, N. S. Godwin, W. A. Richter, C. H. Ziemermann, B. A. Brown, W. E. Ormand, and J. S. Winfield, computer code OXBASH, MSU-NSCL Report No. 524, 1985 (unpublished).
[35] A. Hosaka, K.-I. Kubo, and H. Toki, Nucl. Phys. **A444**, 76 (1985).
[36] H. Mach, E. K. Warburton, R. L. Gill, R. F. Casten, J. A. Becker, B. A. Brown, and J. A. Winger, Phys. Rev. C **41**, 226 (1990).
[37] Chang-hua Zhang, Shun-jin Wang, and Jin-nan Gu, Phys. Rev. C **60**, 054316 (1999).
[38] J. Holden, N. Benczer-Koller, G. Jakob, G. Kumbartzki, T. J. Mertzimekis, K.-H. Speidel, A. Macchiavelli, M. McMahan, L. Phair, P. Maier-Komor, A. E. Stuchbery, W. F. Rogers, and A. D. Davies, Phys. Lett. B **493**, 7 (2000).
[39] J. Holden, N. Benczer-Koller, G. Jakob, G. Kumbartzki, T. J. Mertzimekis, K.-H. Speidel, C. W. Beausang, R. Krücken, A. Macchiavelli, M. McMahan, L. Phair, A. E. Stuchbery, P. Maier-Komor, W. Rogers, and A. D. Davies, Phys. Rev. C **63**, 024315 (2001).
[40] G. Jakob, N. Benczer-Koller, G. Kumbartzki, J. Holden, T. J. Mertzimekis, K.-H. Speidel, R. Ernst, A. E. Stuchbery, A. Pakou, P. Maier-Komor, A. Macchiavelli, M. McMahan, L. Phair, and I. Y. Lee, Phys. Rev. C **65**, 024316 (2002).
[41] G. Jakob, N. Benczer-Koller, J. Holden, G. Kumbartzki, T. J. Mertzimekis, K.-H. Speidel, C. W. Beausang, and R. Krücken, Phys. Lett. B **468**, 13 (1999).
[42] G. Jakob, N. Benczer-Koller, J. Holden, G. Kumbartzki, T. J. Mertzimekis, K.-H. Speidel, R. Ernst, P. Maier-Komor, C. W. Beausang, and R. Krücken, Phys. Lett. B **494**, 187 (2000).
[43] T. Hayakawa, Y. Toh, M. Oshima, A. Osa, M. Koizumi, Y. Hatsukawa, Y. Utsuno, J. Katakura, and M. Matsuda, Phys. Rev. C **67**, 064310 (2003).
[44] T. J. Mertzimekis, Ph.D. thesis, Rutgers University, 2002.
[45] V. Werner, D. Belic, P. von Brentano, C. Fransen, A. Gade, H. von Garrel, J. Jolie, U. Kneissl, C. Kohstall, A. Linnemann, A. F. Lisetskiy, N. Pietralla, H. H. Pitz, M. Scheck, K.-H. Speidel, F. Stedile, and S. W. Yates, Phys. Lett. B **550**, 140 (2002).
[46] S. Kuyucak and A. E. Stuchbery, Phys. Lett. B **348**, 315 (1995).
[47] S. S. Anderssen, A. E. Stuchbery, and S. Kuyucak, Nucl. Phys. **A593**, 212 (1995).
[48] E. D. Davis and P. Navrátil, Phys. Rev. C **50**, 2362 (1994).
[49] F. Brandolini, N. H. Medina, A. E. Stuchbery, S. S. Anderssen, H. H. Bolotin, D. Bazzacco, D. De Acuña, M. De Poli, R. Menegazzo, P. Pavan, C. Rossi Alvarez, and G. Vedovato, Eur. Phys. J. A **3**, 129 (1998).
[50] M. P. Robinson and A. E. Stuchbery, Nucl. Instrum. Methods Phys. Res. A **469**, 469 (2002).